EPR of S_2^- in RbCl and RbBr

1992 J. Phys.: Condens. Matter 4 249

(http://iopscience.iop.org/0953-8984/4/1/035)

J. Phys.: Condens. Matter 4 (1992) 249–256. Printed in the UK

EPR of S_2^- in RbCl and RbBr

F Maes, P Matthys, F Callens†, P Moens and E Boesman
Laboratorium voor Kristallografie en Studie van de Vaste Stof, Rijksuniversiteit Gent, Krijgslaan 281-S1, B-9000 Gent, Belgium

Received 12 June 1991

Abstract. An EPR study of a new S_2^- defect in RbCl is presented. A comparison with the S_2^- centre in RbBr, previously found by Vannotti *et al* is made. For both salts a clearly resolved superhyperfine structure was observed, which has not yet been reported. The interpretation of the spectra was complicated by the simultaneous presence of the ^{85}Rb ($I = 5/2$) and ^{87}Rb ($I = 3/2$) nuclei. An excellent quantitative agreement between simulation and the experimental data was obtained, using only two parameters, i.e. the linewidth for a single superhyperfine component and the ^{85}Rb ($I = 5/2$) splitting. The analysis is based on the interaction of the unpaired electron on the S_2^- ion with four equivalent Rb nuclei. The model is consistent with an S_2^- ion replacing a single Cl^-, respectively Br^-, ion.

1. Introduction

By using an alternative [1] doping procedure our group recently introduced two new chalcogen defect types in several alkali halides [1–7]. We were able to show that new types of X^- and X_2^- (X = S, Se) chalcogen centres are responsible for the EPR spectra. Several models differing in location or environment for these defects are investigated. Recently, we detected a new S_2^- defect in RbCl. In order to find new sulphur defects we also investigated RbBr. We observed the S_2^- ion of Vannotti *et al* [8]. A clearly resolved superhyperfine structure (SHFS) was observed in both crystals, which was not reported in [8] for RbBr:S_2^-.

2. Experimental technique

Single crystals were grown by the Bridgman method [1]. The growth capsule contained RbCl, respectively RbBr powder (p.a. UCB) and about 0.3 wt% of both sulphur and Rb metal (Merck). The alkali halide powder was dried under vacuum at a temperature of 250 °C for one week. The Rb metal and the sulphur were added to the RbCl, respectively, RbBr powder under argon, in a plastic bag (Aldrich Chemie) fitted with gloves. Samples thus grown were x-irradiated at room temperature for typically 30 min with a tungsten anticathode Philips x-ray tube, operated at 60 kV and 40 mW.

† Research Associate of the NFSR (Belgium).

0953-8984/92/010249 + 08 $03.50

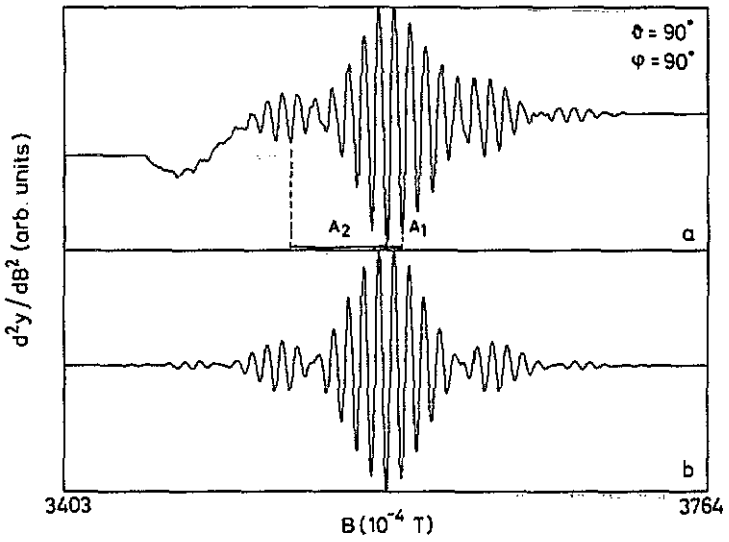

Figure 1. The second derivative EPR spectrum of the S_2^- centre in RbCl with $\boldsymbol{B}$ parallel to ⟨001⟩. The experimental hyperfine pattern (*a*) is compared with a simulation assuming four equivalent Rb nuclei (*b*). The interline field separation A_1 within a group of resonances and the field separation A_2 between the low field and the centre field group is indicated.

EPR spectra were recorded with a Bruker ESP300 X band spectrometer, equipped with an Oxford Instruments ESR10 flow cryostat. The magnetic field was modulated at 100 kHz with a peak-to-peak amplitude of 10^{-4} T. The samples could be rotated about a vertical axis perpendicular to the magnetic field $\boldsymbol{B}$. Crystals cleaved to rotate around a ⟨001⟩ direction and crystals polished to rotate around a ⟨110⟩ direction (only for RbCl) were prepared and an angular dependence was determined for both types of crystals. All spectra were normalized to 9.47 GHz. The best detection conditions were 4 K and 200 mW for the S_2^- in RbBr, in agreement with Vannotti *et al* [8], and 30 K and 1 mW for the S_2^- in RbCl. These detection conditions for the new S_2^- ion in RbCl are similar to those for the S_2^- and Se_2^- ions detected by our group recently in other alkali halides.

3. EPR results and analysis

In figures 1, 2 and 3, typical second derivative EPR spectra of the new S_2^- centre in RbCl are shown. The resonance lines are designated by their polar angles θ and φ. These angles describe the orientation of $\boldsymbol{B}$ with respect to a set of (x, y, z) axes being ([110], [001], [1$\bar{1}$0]). The g values for the new S_2^- defect in RbCl are listed in table 1. The principal axes, corresponding to g_{xx}, g_{yy} and g_{zz}, are orientated along [110], [001] and [1$\bar{1}$0] respectively. A clearly resolved SHFS was seen, which is rarely observed for this class of defects in alkali halides. In figures 1(*a*), 2(*a*) and 3(*a*) one can see typical EPR spectra for this defect. A group of EPR resonances is observed at the centre of the spectrum, this pattern is repeated on both the low- and high-field side. A_1 is the interline field separation and A_2 is the field separation between the low (high) field and the centre field group. In figures 1(*a*), 2(*a*) and 3(*a*) the splittings A_1 and A_2 are indicated. Clearly, the ratio $A_2/A_1 = 6.6$, which seems to be independent of the orientation, is an important

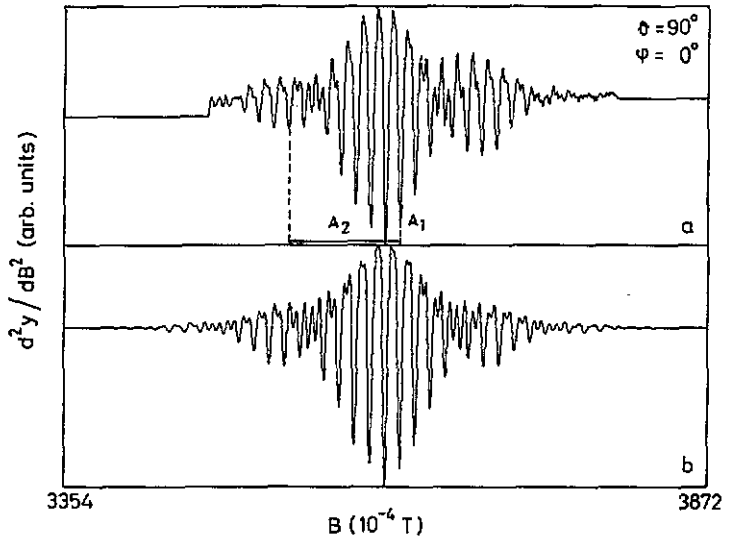

Figure 2. The second derivative EPR spectrum of the S_2^- centre in RbCl with $\boldsymbol{B}$ parallel to ⟨110⟩. The experimental hyperfine pattern (*a*) is compared with a simulation assuming four equivalent Rb nuclei (*b*). The interline field separation A_1 within a group of resonances and the field separation A_2 between the low field and the centre field group is indicated.

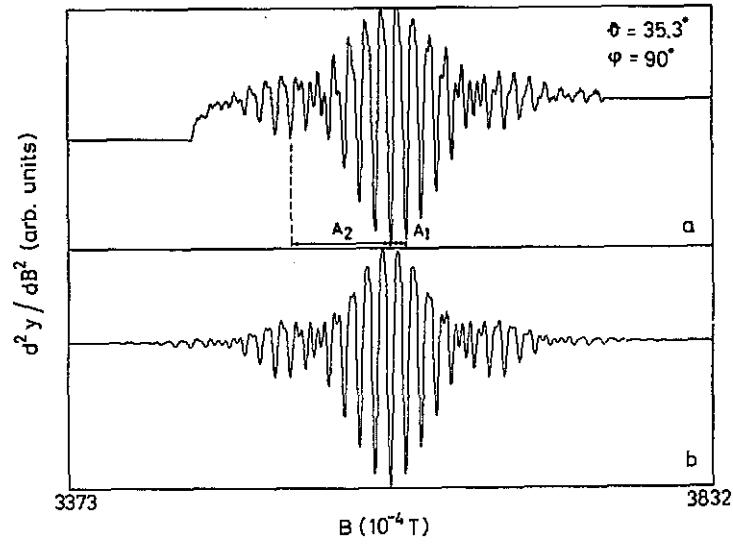

Figure 3. The second derivative EPR spectrum of the S_2^- centre in RbCl with $\boldsymbol{B}$ parallel to ⟨111⟩. The experimental hyperfine pattern (*a*) is compared with a simulation assuming four equivalent Rb nuclei (*b*). The interline field separation A_1 within a group of resonances and the field separation A_2 between the low field and the centre field group is indicated.

experimental parameter characterizing the observed EPR spectra. However, the analysis of the spectra is complicated by the simultaneous presence of ^{85}Rb ($I = 5/2$) and ^{87}Rb ($I = 3/2$). Several configurations of the Rb^+ ions surrounding the S_2^- ions were

Table 1. g tensor of the S_2^- defect in NaCl, KCl, RbCl, RbBr and RbI.

	⟨110⟩	⟨001⟩	⟨1$\bar{1}$0⟩	
	g_{xx}	g_{yy}	g_{zz}	Ref
NaCl	2.0107	1.9860	2.2531	[1, 3]
KCl	1.9708	1.9491	2.4548	[2, 3]
RbCl	1.8728	1.8881	2.6515	this paper
RbBr	1.7447	1.7571	2.8936	[8]
RbI	1.2895	1.2969	3.3595	[8]

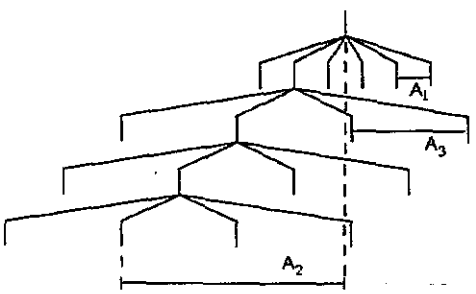

A_1 = Spl($^{85}Rb_{5/2}$)
A_3 = Spl($^{87}Rb_{3/2}$)
A_2 = 3/2 A_1 + 3*1/2 A_3

Figure 4. The diagram explains how four Rb^+ ions give rise to the ratio A_2/A_1.

tried for computer simulations. In doing so we noticed that simulations assuming an even number (2, 4, 6) of equivalent Rb nuclei give rise to a pattern that qualitatively agrees with the experimental spectra: the ratio of the field distance between the three main groups of lines (A_2), to the field distance between the individual lines (A_1) also equals 6.6. The best results were obtained using four equivalent Rb nuclei. The diagram in figure 4 explains how four Rb^+ ions give rise to the ratio A_2/A_1. This diagram is a part of the total stick diagram shown in figure 5. According to figure 4 one can calculate the ratio A_2/A_1:

$$A_1 = \mathrm{Spl}(^{85}\mathrm{Rb}_{5/2}) \qquad A_3 = \mathrm{Spl}(^{87}\mathrm{Rb}_{3/2})$$

$$A_2 = 3/2\,A_1 + 3(1/2\,A_3)$$

$$A_2/A_1 = 3/2(1 + A_3/A_1) = 3/2(1 + g_{n(3/2)}/g_{n(5/2)}) = 3/2(1 + 3.3889) = 6.583$$

where Spl denotes splitting and g_n is the nuclear g factor.

The agreement between the calculated and the experimental value of A_2/A_1 is excellent.

In figure 5 a stick diagram is presented with the first order positions and the intensities of every peak. This diagram is characteristic for four equivalent Rb^+ ions. In table 2 some results from the fittings are presented (the splitting mentioned pertains to ^{85}Rb ($I = 5/2$)). In figures 1(b), 2(b) and 3(b) the results of the computer simulations are presented. Only two parameters were used for these simulations, i.e. the linewidth for a single superhyperfine component and the splitting due to the ^{85}Rb ion. The splitting caused by

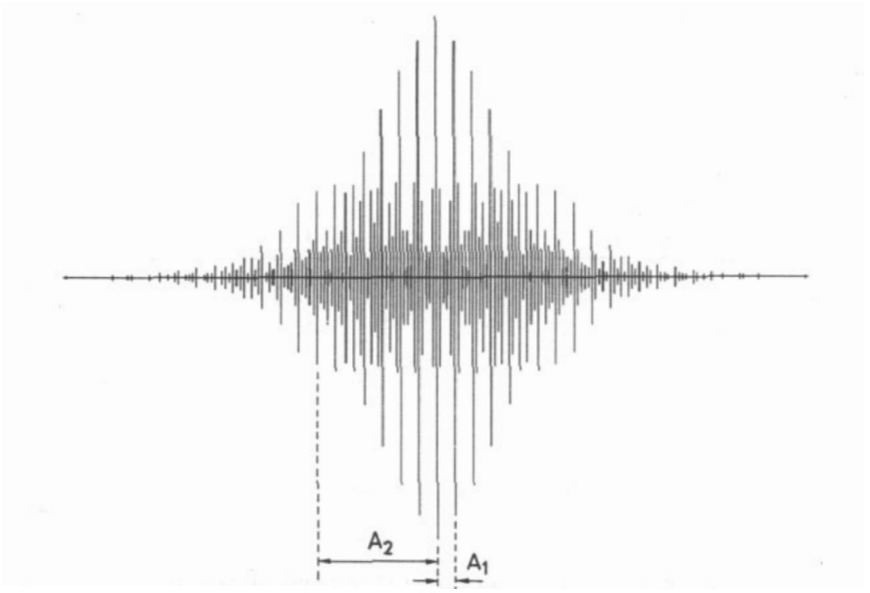

Figure 5. A characteristic stick diagram for four equivalent Rb nuclei. The first order position and the intensity of every peak is indicated. The interline field separation A_1 within a group of resonances and the field separation A_2 between the low field and the centre field group is indicated.

Table 2. Computer simulation parameters for RbCl, the splitting mentioned is the one of ^{85}Rb (in 10^{-4} T).

	Splitting	Linewidth
[001]	8.25	4.05
[110]	12.16	4.65
[111]	10.73	4.46

the ^{87}Rb ion is $g_{n(3/2)}/g_{n(5/2)}$ times larger than the splitting due to the ^{85}Rb ion. The agreement between the computer simulations, figures 1(*b*), 2(*b*) and 3(*b*), and the experimental spectra, figures 1(*a*), 2(*a*) and 3(*a*), is excellent.

We also investigated RbBr crystals in order to find new sulphur defects. We observed the S_2^- ion of Vannotti *et al* [8]. In contradiction with their measurements we detected SHFS. The results of our measurements and of the computer simulations are presented in figures 6 and 7. The determined ^{85}Rb splittings and linewidths can be found in table 3. Again four equivalent Rb^+ ions were used to explain the spectra.

4. Discussion

The assumption that the spectrum in RbCl is due to an S_2^- ion is supported by the analysis of the *g* tensor. Applying the theory for O_2^- (or S_2^- or Se_2^-) derived in [9], the *g* tensor

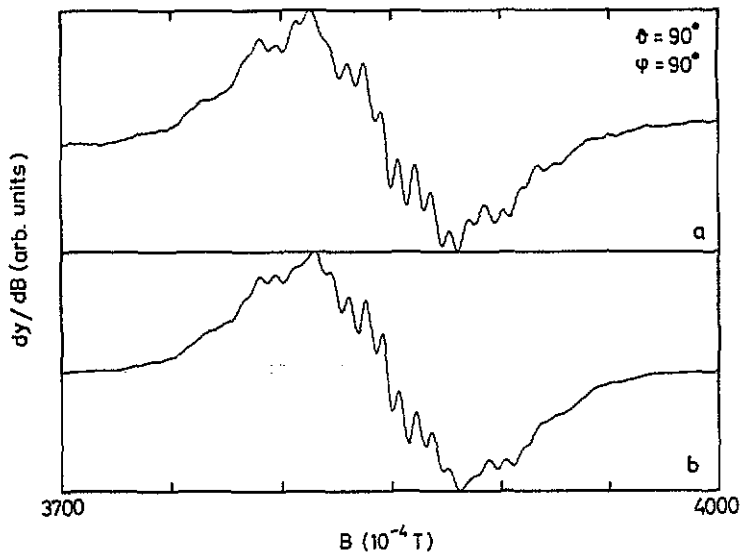

Figure 6. The EPR spectrum of the S_2^- centre in RbBr with B parallel to ⟨001⟩. The experimental hyperfine pattern (*a*) is compared with a simulation assuming four equivalent Rb nuclei (*b*).

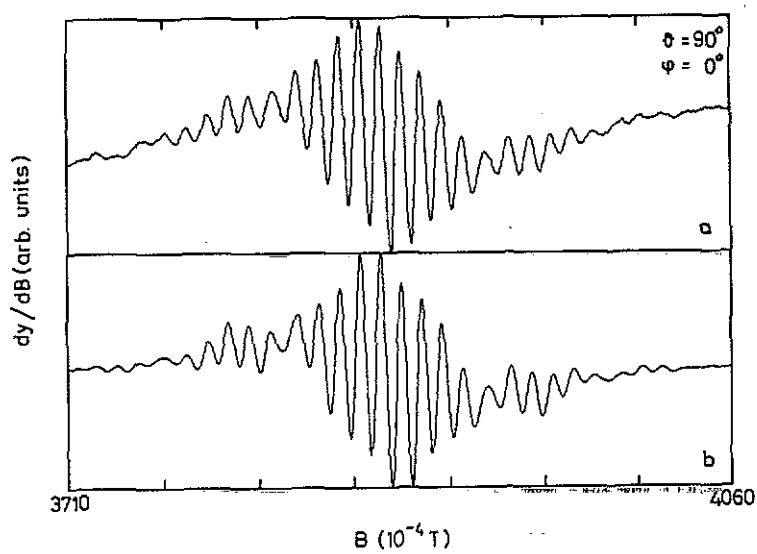

Figure 7. The EPR spectrum of the S_2^- centre in RbBr with B parallel to ⟨110⟩. The experimental hyperfine pattern (*a*) is compared with a simulation assuming four equivalent Rb nuclei (*b*).

principal values for the S_2^- defect in RbCl are given by

$$g_{xx} = g_e \cos 2\alpha + (\cos 2\alpha - 1 + \sin 2\alpha)\lambda/E$$

$$g_{yy} = g_e \cos 2\alpha + (\cos 2\alpha + 1 - \sin 2\alpha)\lambda/E$$

$$g_{zz} = g_e + 2l \sin 2\alpha.$$

In what follows the energy levels will be classified according to the irreducible

Table 3. Computer simulation parameters for RbBr, the splitting mentioned is the one of ^{85}Rb (in 10^{-4} T).

	Splitting	Linewidth
[001]	7.34	7.98
[110]	10.44	7.67

representations of $D_{\infty h}$ (free molecular ion) and D_{2h} (molecular defect). Here $g_{xx} < g_{yy}$, which means that the unpaired electron is placed in the Γ_2^+ (D_{2h})-state [10]. In these equations l represents a correction to the angular momentum caused by the crystal field (l is unity for the free molecular ion), λ is an effective spin–orbit splitting of the molecule in the crystal field, Δ ($\lambda/\Delta = \tan 2\alpha$) is the crystal field splitting parameter and E is the energy difference of the $3p\,\Pi_g$ ground state $[\Pi_g^x(D_{\infty h}) \rightarrow \Gamma_2^+(D_{2h})$; $\Pi_g^y(D_{\infty h}) \rightarrow \Gamma_4^+(D_{2h})]$ and the $3p\,\Sigma_g$ state $[\Sigma_g(D_{\infty h}) \rightarrow \Gamma_1^+(D_{2h})]$. For more details we refer to [9]. The equations contain three independent parameters which can be calculated to be

$$\lambda/\Delta = 0.3839 \qquad \lambda/E = 0.0119 \qquad \text{and } l = 0.9058.$$

The conclusions that the observed defect in RbCl is an S_2^- defect is also supported by comparison with g tensor data of some other S_2^- defects. By inspection of the values summarized in table 1, the S_2^- ion in RbCl fits in nicely both with the series of S_2^- centres in other alkali chlorides (divacancy) and rubidium halides (monovacancy). The assignation of the other S_2^- defects was supported by the analysis of the hyperfine data. Finally, the attribution of the observed defects to an S_2^- ion is supported by the fact that for the five mentioned species the theory given above accounts well both for the g tensor data and for the A tensor data (where available). We conclude that the observed defect in RbCl is an S_2^- ion.

The Rb superhyperfine splittings in RbBr are smaller than in RbCl. This is probably due to the larger distance between the Rb^+ ions and the S_2^- centre. The approximate doubling in linewidth in RbBr compared with RbCl is possibly due to the larger g_n factors of Br: the g_n factors of Br are approximately three times larger than those of Cl but this effect is partially compensated as the distance between the S_2^- and the surrounding halogen ions is larger in RbBr than in RbCl.

The observed spectra can be explained with four equivalent Rb nuclei, as already stated above. The problem of the location of the S_2^- ions in RbCl and RbBr remains to be solved. In the literature two models have been presented for similar chalcogen defects:

(i) an X_2^- ion replacing one halide ion, as shown in figure 8(a).
(ii) an X_2^- ion replacing two halide ions, as shown in figure 8(b).

According to Vannotti *et al* [8], the S_2^- ion in RbBr substitutes for one halide ion. They proposed this model in analogy with the O_2^- ion detected by Zeller *et al* [9]. In contradiction with Zeller *et al*, Vannotti *et al* did not observe any SHFS for their S_2^- ions.

The SHFS that we observed in RbCl and RbBr for the S_2^- ions is analogous with the SHFS of the O_2^- ions detected by Zeller *et al* [9]. For both defects one has a well-resolved SHFS in the directions $B \| x$ and $B \| y$ which can be explained with four equivalent Rb nuclei. The resonance in the direction $B \| z$ was not well resolved due to background signals. Using the model of figure 8(a) one can very easily verify that for $B \| x$ and $B \| y$

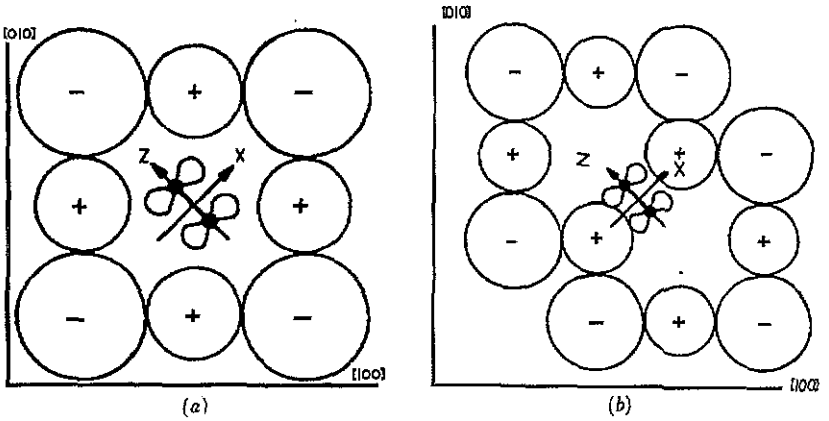

Figure 8. An S_2^- ion replacing one halide ion in RbCl (*a*); an S_2^- ion replacing two halide ions in RbCl (*b*).

the four Rb nuclei in the (001) plane are responsible for the spectra. With the model of figure 8(*b*) one cannot explain how the SHFS arises from four equivalent Rb nuclei. Consequently, we believe that the S_2^- ions described here substitute for one Cl^- ion in RbCl and for one Br^- ion in RbBr.

References

[1] Matthys P, Callens F and Boesman E 1983 *Solid State Commun.* **45** 1
[2] Callens F, Matthys P and Boesman E 1983 *Phys. Status Solidi* b **118** K35
[3] Callens F, Maes F, Matthys P and Boesman E 1989 *J. Phys.: Condens. Matter* **1** 6921
[4] Matthys P, Maes F, Callens F and Boesman E 1990 *Solid State Commun.* **75** 17
[5] Maes F, Callens F, Matthys P and Boesman E 1990 *Phys. Status Solidi* b **161** K1
[6] Maes F, Callens F, Matthys P and Boesman E 1990 *J. Phys. Chem. Solids* **51** 1289
[7] Maes F, Callens F, Matthys P and Boesman E 1991 *Radiation Effects and Defects in Solids* **116** 283
[8] Vannotti L E and Morton J R 1967 *Phys. Rev.* **161** 282
[9] Zeller H R and Känzig W 1967 *Helvetica Physica Acta* **40** 845
[10] Koster G F, Dimmock J O, Wheeler R G and Statz H 1963 *Properties of the Thirty-Two Point Groups* (Cambridge: MIT Press) p 39